RESEARCH ARTICLE

Check for updates

Acid–base interactions in luminescent silver(I) and gold(I) complexes with phosphine–phosphinate/phosphinite ligands

Mariia Beliaeva,[a] Andrey Belyaev, [ID] [a] Henna Korhonen,[a] Ondrej Mrózek, [ID] [b] Janne Jänis, [ID] [a] Andreas Steffen [ID] *[b] and Igor O. Koshevoy [ID] *[a]

Hybrid phosphines with anionic hard donor functions can be used to create an adaptable ligand environment for soft late transition metals. Herein, we show that the change of coordination of a diphosphine–phosphinic acid (**P³OO**H) in response to acid–base interactions or hydrogen bonding results in structural transformations of a disilver complex [Ag₂(**P³OO**)₂] (**1**) to give solvated and protonated derivatives [Ag₂(**P³OO**H)₂]²⁺ (**2**) and [Ag₃(**P³OO**)₃H]⁺ (**3**), accompanied by the alteration of the quantum yield of the solid-state photoluminescence from 0.06 up to 0.69. The related diphosphine–phosphide oxide complexes [M₂(**P³O**)₂] (M = Ag, Au) are oxidized to phosphinate compounds **2** and non-luminescent [Au₂(**P³OO**)₂H]⁺ (**5**) in the presence of triflic acid. Alternatively, [Au₂(**P³O**)₂] readily accommodates an additional gold(I) ion to yield a trinuclear cluster [Au₃(**P³O**)₂]⁺ (**6**), which is brightly sky-blue phosphorescent in the crystalline state (Φ_{em} = 0.76). The phosphide oxide group ⁻P=O in **6** is stable towards oxidation under acidic conditions in solution but undergoes protonation that results in two orders of magnitude (>170-fold) increase of the emission intensity. Complex **6** acts as a guest in the crystalline matrix of **5** due to their structural similarity and affords solid solutions with bright luminescence at a doping content of 1–2%.

Introduction

The acid–base stimuli have a pronounced effect on the photophysical behavior of a variety of chromophore species. Distinct responses in absorption and luminescence to protonation/deprotonation or alteration of hydrogen bonding are conventionally attained in donor–acceptor (D–A) organic molecules by modulating intramolecular charge transfer (ICT) or photoinduced electron transfer (PET). These phenomena have been widely employed in the development of numerous chemosensing and bioimaging probes, switchable and responsive materials.[1–9]

A similar strategy has been applied to photoemissive transition metal complexes by utilizing the ligands decorated with donor/acceptor functions (hydroxyl, carboxyl, amines/N-heterocycles *etc.*) capable of reversible interaction with protic acids and bases. The involvement of the metal and ligand orbitals into electronic transitions offers a selection of excited states (ligand or metal centered (LC/MC), intraligand (IL)/metal to ligand (ML)/ligand to metal (LM)/ligand to ligand

(LL) charge transfers). Their energies, mixing, population, and deactivation are defined by the nature of the metal ion and acid–base reactivity. A diversity of possible scenarios can be illustrated by tetrazolate d⁶ complexes of Re(I), Ru(II) and Ir(III), which demonstrate hypsochromic shift/enhanced intensity (Re), bathochromic shift/change of the excited state (Ir), and quenching of the emission (Ru) upon protonation.[10] Such characteristics allow the use of luminescent transition metal complexes as sensors for pH,[11–17] acid–base vapors,[18–20] and metal ions,[21] receptors for anions,[22,23] and photodynamic therapy agents.[24]

Interactions with acids and bases can influence the physical properties of metal complexes not only by electronic means of reactive functions tailored to the metal-coordinated ligands, but also through the modulation of non-covalent interactions, for instance hydrogen or metal···metal bonding. Interesting cases of pH-responsive supramolecular aggregates were described for square planar platinum(II) complexes. Their luminescence behavior strongly depends on the intermolecular arrangement, governed by Pt···Pt and π–π stacking interactions. These can be amended upon acid–base treatment of compounds containing ligands with hydrogen bond active sites.[25–28] In a broader view, incorporation of H-bonding groups into complexes, which have a tendency for metallophilicity-driven assembly (*i.e.* primarily those of Pt(II), Au(I)), leads

[a]Department of Chemistry and Sustainable Technology, University of Eastern Finland, Yliopistokatu 7, Joensuu, 80101, Finland. E-mail: igor.koshevoy@uef.fi
[b]Department of Chemistry and Chemical Biology, TU Dortmund University, Otto-Hahn-Str. 6, 44227 Dortmund, Germany. E-mail: andreas.steffen@tu-dortmund.de

This journal is © the Partner Organisations 2026

Inorg. Chem. Front., 2026, **13**, 511–524 | 511

to the competition or interplay of weak forces and offers rich opportunities for the design of luminescent systems with dynamic or chromic behavior.[29–36]

Furthermore, a change in optical properties might arise from external perturbation of intramolecular ligand to metal coordination or reorganization of the ligand sphere. Flexible binding can be achieved for hybrid hemilabile ligands, *i.e.* those simultaneously possessing electronically different donor groups bound to the metal center with different strengths. This type of ligands showing variable coordination has found applications in catalysis and sensing.[37–39] Notably, an adaptable ligand environment, which is regulated by acid–base interactions or hydrogen bonding and producing detectable photophysical changes, remains virtually unexplored among transition metal complexes.[40,41] Nevertheless, a change in coordination mode of a loosely binding function upon interactions with protic and Lewis acids and particularly the related structural transformations are likely to have a substantial influence on the composition of frontier molecular orbitals, energies of electronic transitions, and the excited state properties.

In our previous results on phosphine–phosphine oxide derivatives, we have shown that the neutral P=O moiety interacts with coinage metals at a moderate strength (Cu(I) > Ag(I) > Au(I)),[42] while the deprotonated secondary oxide motif ($^-$P=O) of bis(2-(diphenylphosphaneyl)phenyl)phosphine oxide (HP^3O) forms H-bonds with a clear impact on the photophysical characteristics of disilver(I) and digold(I) complexes [M$_2(P^3O)_2$].[43,44] In this work, we have selected a chelating phosphine comprising phosphinic acid as a concept of an adaptable ligand (Fig. 1), with an aim to investigate its coordination chemistry towards d[10] coinage metal ions and the photophysical behavior of the corresponding compounds. This choice was dictated by the following reasons: (i) numerous phosphine complexes of Cu(I), Ag(I) and Au(I) show rich luminescence behavior;[45–49] (ii) phosphinate/phosphonate (R$_2$PO$_2^-$/RPO$_3^{2-}$) groups are prone to protonation and hydrogen bonding[50,51] and as hard O-donors are expected to have

weaker affinity to d[10] coinage metal ions in comparison to phosphines; (iii) the variable coordination number of coinage metals can adjust to the ligand environment;[52] (iv) there have been only a few reports on mixed phosphine–phosphinic/phosphonic acids (or salts)[53–55] and their coordination complexes (Fig. 1).[56–59]

We now demonstrate that using a novel diphosphine–phosphinate ligand, bis(2-(diphenylphosphaneyl)phenyl)phosphinic acid (P^3OOH), allows for the preparation of structurally flexible silver(I) and gold(I) complexes, the molecular arrangement and photoluminescent behavior of which are affected by the anionic R$_2$POO$^-$ part acting as a proton acceptor.

Simultaneously, we further studied the reactivity of compounds [M$_2(P^3O)_2$] (M = Ag(I), Au(I))[43,44] towards acids. Thus, a strong protic acid promotes a facile transformation of a phosphinite (phosphide–oxide) group $^-$P(O)R$_2$ into a phosphinate function R$_2$POO$^-$. On the other hand, [Au$_2(P^3O)_2$] readily adds the Au(I) ion (Lewis acid), resulting in the expansion of the cluster framework that stabilizes the phosphide oxide motif $^-$P=O and makes it sensitive to the protonation with a distinct optical response.

## Results and discussion

Syntheses

The target ligand P^3OOH was synthesized *via* the lithiation of (2-bromophenyl)diphenylphosphine[61] and coupling with a stoichiometric amount of ethyl dichlorophosphate to afford intermediate diphosphine–ethyl phosphinate (P^3OOEt, Scheme 1) in a good yield of 74% (see experimental details in SI). Its subsequent hydrolysis with hydrochloric acid and alkalinization with sodium carbonate gives the corresponding salt P^3OONa, the treatment of which with an equimolar amount of hydrochloric acid in methanol–water solution readily converts it into the acidic form P^3OOH with an overall yield of 87%.
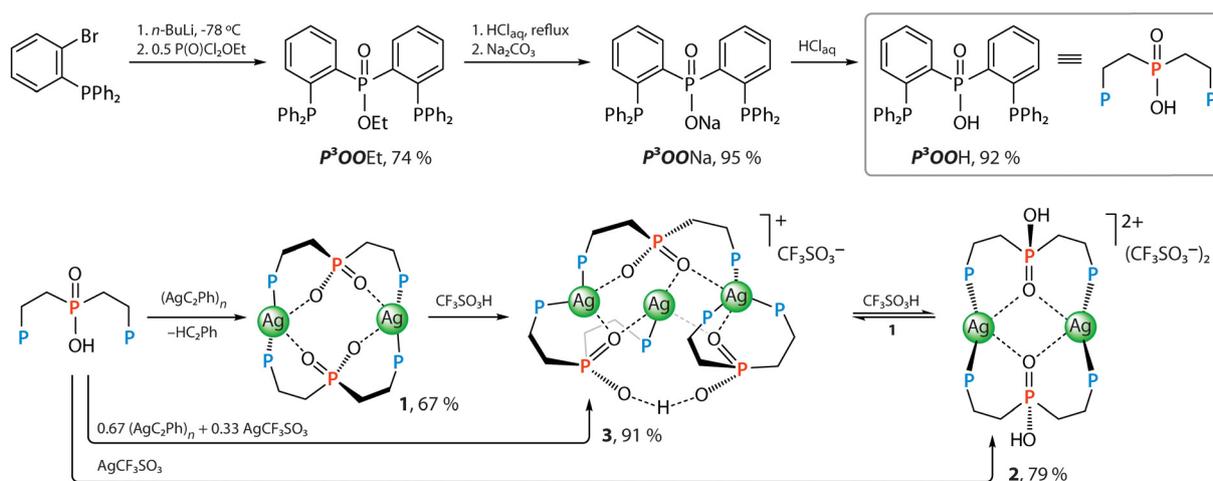
The reaction of silver(I) acetylide (AgC$_2$Ph)$_n$[62] with P^3OOH under ambient conditions results in substitution of the hydrocarbon ligand and produces colorless neutral dimetallic complex [Ag$_2(P^3OO)_2$] (**1**), which can be conveniently isolated as a methanol solvate. The use of silver triflate AgCF$_3$SO$_3$ instead of (AgC$_2$Ph)$_n$ yields pale yellowish bis-protonated cationic derivative [Ag$_2(P^3OO$H)$_2$](CF$_3$SO$_3$)$_2$ (**2**, Scheme 1). Alternatively, **2** can be generated from **1** by adding a slight excess of triflic acid. In attempt to prepare the monoprotonated congener, a trimetallic cluster [Ag$_3(P^3OO)_3$H](CF$_3$SO$_3$) (**3**) was identified as the only new product, which can be obtained by reacting the phosphine P^3OOH with (AgC$_2$Ph)$_n$ and AgCF$_3$SO$_3$ in 3 : 2 : 1 molar ratio.[43] Analogous gold(I) compounds, however, are not formed in the reaction of the corresponding (AuC$_2$Ph)$_n$ acetylide with P^3OOH, which yields poorly soluble products probably having a polymeric nature.

The easy protonation of a coordinated phosphinate group POO$^-$ in **1** prompted us to probe the behavior of the congener phosphine–phosphide oxide complexes [M$_2(P^3O)_2$], which are derived from the (o-Ph$_2$PC$_6$H$_4$)$_2$P(O)H (HP^3O) ligand (M = Ag,[43]
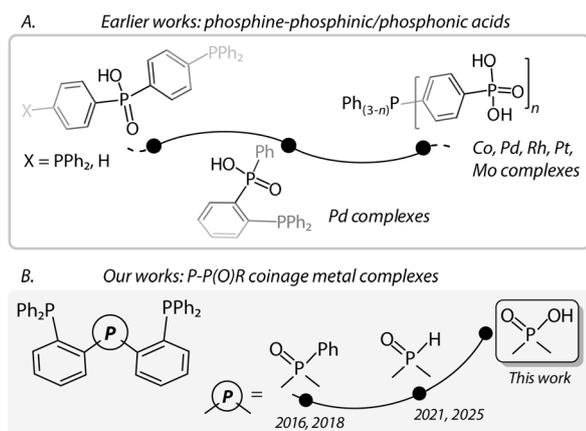
Fig. 1 Examples of (A) phosphine–phosphinic/phosphonic acid ligands;[53–55] (B) chelating diphosphines with P=O functions used in our works.[42–44,60]

512 | *Inorg. Chem. Front.*, 2026, **13**, 511–524

This journal is © the Partner Organisations 2026

Scheme 1 Syntheses of ligand P^3OOH and complexes **1–3**.

Au[44]), under acidic conditions. We have shown previously that the [Ag$_2$(P^3O)$_2$] adds an equimolar amount of HCl to give [Ag$_2$(P^3O)$_2$H(μ-Cl)] as a result of hydrohalogenation.[43] The digold relative [Au$_2$(P^3O)$_2$] reacts with two equivalents of HCl yielding yellow-orange doubly protonated species [Au$_2$(HP^3O)] Cl$_2$ (**4**), which also can be obtained from the HP^3O phosphine and [Au(tht)Cl] (tht = tetrahydrothiophene) in 82% yield, Scheme 2 and the SI. Interestingly, applying stronger triflic acid in aerated solution quickly oxidizes the phosphide-oxide groups to the phosphinates, converting [M$_2$(P^3O)$_2$] into the aforementioned bis-protonated complex **2** and monoprotonated [Au$_2$(P^3OO)$_2$H]CF$_3$SO$_3$ (**5**) for M = Ag and Au, respectively (Scheme 2). This transformation of the metal-bound phos-
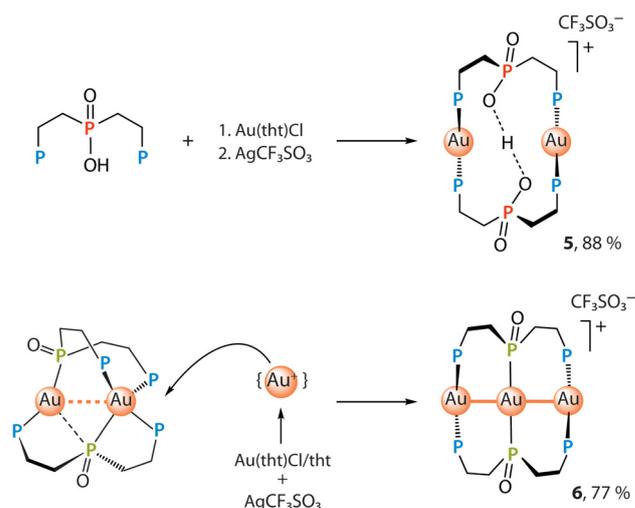
phine, i.e. HP^3O + $\frac{1}{2}$O$_2$ → P^3OOH, occurs if HP^3O is reacted with silver triflate, or when the chloride is replaced by the triflate in **4** in an aerated solution. Both pathways leading to complexes **2** and **5** (Scheme 2) can be considered as the protonation of the oxygen atom in the M–PR$_2$=O fragment ($\lambda^5\sigma^4$-P configuration) by a strong acid that likely increases the contribution of the resonance form M$^+$–PR$_2$–OH ($\lambda^4\sigma^4$-P) having phosphinous acid ligand. This, in turn, enhances the nucleophilicity of the central phosphorus atom and makes it more reactive towards molecular oxygen.

A more efficient synthesis of colorless complex **5** involves the reaction of P^3OOH ligand with [Au(tht)Cl] and subsequent removal of the chloride with AgCF$_3$SO$_3$ (Scheme 3).

Notably, an acid-mediated oxidation of [Au$_2$(P^3O)$_2$] produces **5** as a yellowish crystalline material **5***, which contains **5** as a main component accompanied by a very minor (ca. 1–2%) but systematically reproduced admixture of a trigold cluster
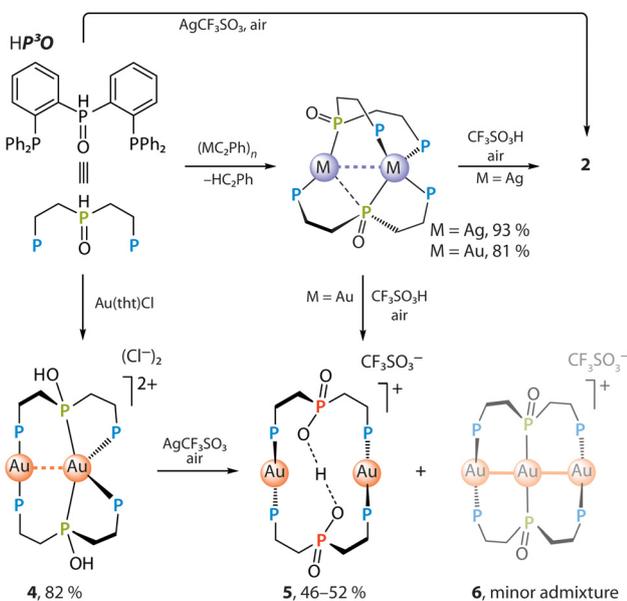
Scheme 2 Preparation of phosphinate complexes **2** and **5** via acid-mediated oxidation of the $^-P^3O$ phosphine–phosphide oxide ligand.

Scheme 3 Selective syntheses of complexes **5** and **6**.

This journal is © the Partner Organisations 2026

Inorg. Chem. Front., 2026, **13**, 511–524 | 513

$[Au_3(\textbf{\textit{P}}^3\textbf{\textit{O}})_2]CF_3SO_3$ (**6**), see the discussions of the X-ray data and solid-state photophysical properties below. The ability of the digold complex to accept an additional metal ion likely stems from coordinative saturation of one of the gold centers being in a pseudotetrahedral environment of four P-donors.

Curiously, the trigold species **6** initially evaded detection: none of the conventional characterization techniques (XRD, NMR and mass-spectrometry, elemental analysis) gave a clear indication of its presence. It was only when two separate reactions leading to **5*** and **5** (Schemes 2 and 3) yielded crystals of distinctly different colors and luminescence behavior that required an explanation. This anomaly was not resolved by repeated crystallizations, but column chromatography performed on **5*** (silica gel, dichloromethane–methanol, 95 : 5 v/v) led to a substantial enrichment of the mixture with elusive trigold complex **6**, increasing its content to nearly 30% (*vide infra*).

Yellow-greenish cluster **6** is readily obtained in 77% yield from $[Au_2(\textbf{\textit{P}}^3\textbf{\textit{O}})_2]$ and labile species $[Au(tht)_n]CF_3SO_3$ generated *in situ* (Scheme 3 and the SI). In contrast to the parent $[Au_2(\textbf{\textit{P}}^3\textbf{\textit{O}})_2]$ compound, complex **6** is stable in the presence of a strong acid, showing no visible signs of oxidation of the phosphide oxide moiety.

No silver analogue of **6** was formed in the reaction of $[Ag_2(\textbf{\textit{P}}^3\textbf{\textit{O}})_2]$ with silver triflate, which proceeds non-stoichiometrically, giving a mixture of products.

Structural and spectroscopic characterization

The ligand $\textbf{\textit{P}}^3\textbf{\textit{OO}}$H (Fig. S1) and complexes **1–6** were structurally analyzed; the crystal data and selected parameters are listed in Tables S1–S10. Complex **1** readily crystallizes in the presence of methanol to give solvate **1**(MeOH), Fig. 2. This form reveals a centrosymmetric molecule with a compact $\{Ag_2O_2\}$ core composed of two metal atoms and asymmetrically bridging oxygens of the μ_2:O_1,O_1 R_2POO^- groups. The Ag–O distances (2.361(1) and 2.499(1) Å, Table S3) are comparable to

those for related compounds bearing phosphinate/phosphonate ligands.[63–65] The second oxygen atom of the acidic function does not participate in binding to the metal and is involved in PO⋯H–OMe hydrogen bonding with methanol molecules at the PO⋯O_{MeOH} distances of 2.641(3) and 2.728(3) Å. The four-coordinate environment of the silver ions is completed by two Ag–P bonds (2.399(4) and 2.438(5) Å), their lengths are also typical for silver phosphine derivatives.[42,43,63,66] The separation between metal centers in **1** (MeOH) exceeds 3.7 Å, which implies no appreciable argentophilic interactions.[67,68]

Structurally different modifications, **1**(X/H$_2$O) (X stands for unresolved disordered solvent) and solvent-free **1**, were obtained from dichloromethane/diethyl ether mixture (Fig. 2 and S2). The latter species requires the use of dry solvents and is difficult to reproduce in a phase-pure form. In both **1** (X/H$_2$O) and **1**, the phosphinate anion bridges the metal centers in a μ_2:O_1,O_2 fashion, utilizing two oxygen atoms, resulting in an 8-membered metallacycle with chair-like conformation. The silver ions exhibit a heavily distorted tetrahedral coordination geometry, similar to that in **1**(MeOH), including the Ag–O and Ag–P bond lengths (Table S4 and S5). **1**(X/H$_2$O) contains a fraction of water molecule (*ca.* 0.3) bound to each metal that induces a disorder of the $\{C_6H_4–POO^-\}$ fragment and affects the Ag–O connectivity (Fig. S2).

All three forms **1**, **1**(MeOH) and **1**(X/H$_2$O) crystallize in the same type of space group ($P\bar{1}$) with unit cells of comparable size (Table S1), which points to a possibility of accessible phase transitions. Thus, drying pristine methanol solvate **1** (MeOH) under ambient conditions leads to rapid loss of *ca.* 50% of crystallization solvent (4 out of 8 molecules found in the unit cell according to elemental analysis), apparently which is not involved in hydrogen bonding and occupies the space voids around the molecules of the complex (Fig. S3). This transition gives intermediate phase **1′**(MeOH) with distinct photophysical properties (see discussion below). Further
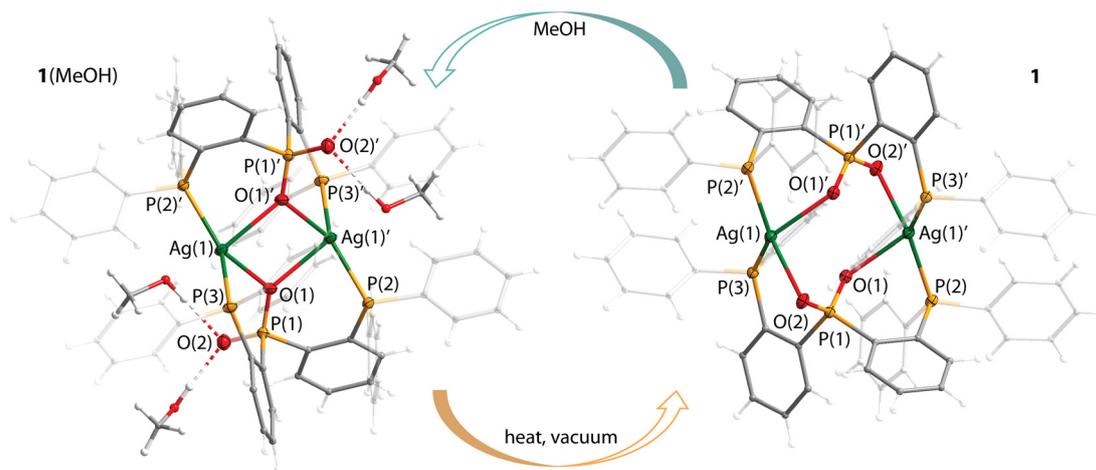
Fig. 2 Molecular views of methanol solvate **1**(MeOH) and solvent-free forms of complex **1** obtained from SC-XRD studies (displacement ellipsoids of non-carbon atoms are shown at the 50% probability level).

514 | *Inorg. Chem. Front.*, 2026, **13**, 511–524

This journal is © the Partner Organisations 2026

vacuum drying at 473 K transforms **1**′(MeOH) into solvent-free material **1** as confirmed by powder X-ray diffraction patterns (Fig. S4). Semi-solvated compound **1**′(MeOH) can be restored by exposing powder sample **1** to methanol vapors.

The molecular configuration of doubly protonated **2** resembles that of **1**(MeOH) and features a nearly flat $\{Ag_2O_2\}$ fragment possessing tetracoordinate silver ions (Fig. 3, Table S6). The short separations between the oxygen atoms of the phosphinate and triflate anions ($d(O\cdots O) = 2.565(7)$ Å) evidence for efficient PO–H⋯OS interactions engaging the acidic residues. Comparable geometry and structural parameters of the $\{Ag_2O_2\}$ core in **2** and **1**(MeOH) manifest that protonation of the phosphinate groups and POO⋯H–OMe hydrogen bonding have a similar effect on the coordination mode of the R_2POO groups, both causing the formation of four-membered metallocycles.

Monocationic complex **3** is constructed of three nonequivalent phosphine ligands and three silver ions, all found in different four-coordination environments $\{AgP_xO_{4-x}\}$, $x = 1–3$, Fig. 3. The assembly of **3** is evidently driven by favorable hydrogen bonding $O(4)\cdots H\cdots O(6)$ ($d(O\cdots O) = 2.445(7)$ Å, Table S7) between two phosphinate groups due to partial protonation. Variable coordination of silver ions and dynamic metal–P/O interactions are other necessary factors, which allow redistribution of the ligand sphere occurring upon formation of **3**.

In a CD_2Cl_2 solution, the $^{31}P\{^1H\}$ spectrum of **1** at 293 K displays two broad resonances (Fig. S4), which indicate substantial structural non-rigidity at room temperature. The unresolved singlet at 26.2 ppm is assigned to acidic phosphorus atom, the high field signal of twice larger integral intensity can be interpreted as two doublets (5.0 and 3.7 ppm, $^1J_{PAg}$ ca. 230 Hz). This pattern arises from nonequivalent phosphine motifs in the absence of significant phosphorus–phosphorus coupling that might occur due to intramolecular dynamics and/or dissociation of a dimeric structure into mononuclear fragments. Addition of methanol to a dichloromethane solution of **1** visibly sharpens the signals and slightly shifts them

to low field region that is tentatively attributed to the formation of hydrogen bonding with protic solvent (Fig. S5).

The protonated derivative **2** undergoes dissociation in a CD_2Cl_2/MeOD-d_3 mixture under ambient conditions and has to be stabilized by adding some triflic acid (Fig. S5). The set of sharp signals consisting of a singlet at 43.4 ppm (POOH) and doublets at 14.3 ppm (–PPh$_2$; two isotopomers $^1J_{PAg} = 339$ and 392 Hz for ^{107}Ag and ^{109}Ag) can be assigned to a symmetrical mononuclear species $[Ag(\boldsymbol{P^3OO}H)]^+$. The broad dominating resonances form the pattern, similar to that of complex **1** but shifted to a low field region that presumably corresponds to binuclear compound being in dynamic equilibrium with triflic acid. The ESI$^+$ mass spectrum of **2** displays the main signal of $[Ag(\boldsymbol{P^3OO}H)]^+$ ion (Fig. S6) that confirms easy fragmentation of the dimeric structure.
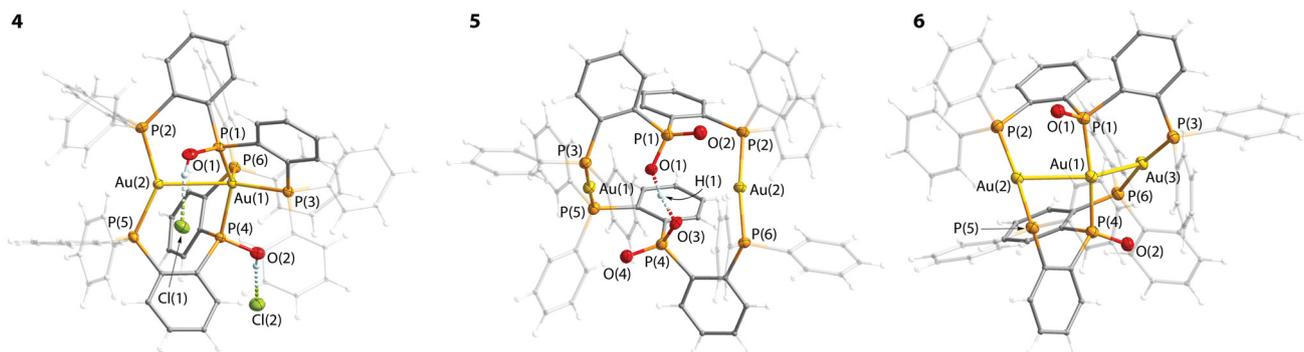
Cluster **3** is rigid in solution in the NMR timescale at ambient conditions. Its phosphorus spectrum exhibits three narrow resonances of equal intensities in the range 31.5–28.8 ppm (Fig. S5), which belong to three different POO$^-$ groups found in crystallographically characterized molecule. The multiplets spanning from 6.1 to −5.7 ppm originate from six different –PPh$_2$ fragments connected to three silver atoms that gives a complicated spin system producing multiple P–^{107,109}Ag and P–P couplings. The presence of the molecular ion of **3** in solution is corroborated by the dominating signal of a doubly charged cation at $m/z = 1060.0$ corresponding to the adduct $[3 + K]^{2+}$ (Fig. S6).

The structure of the intermediate gold complex **4** (Fig. 4 and Table S8) implies the protonation of the phosphide oxide groups, which seemingly form the O–H⋯Cl$^-$ hydrogen bonds with chloride anions ($d(O\cdots Cl) = 2.880(9)–2.926(7)$ Å). Both P(OH) functions of phosphine ligands in **4** are bound to the same gold center. Contrarily, the phosphines in the non-protonated parent compound $[Au_2(\boldsymbol{P^3O})_2]$ have a head-to-tail orientation.[44] The gold atoms in **4** are found in two- and four-coordination environments completed by the P-donor groups. These are supplemented by a short Au–Au contact (2.8615(6)
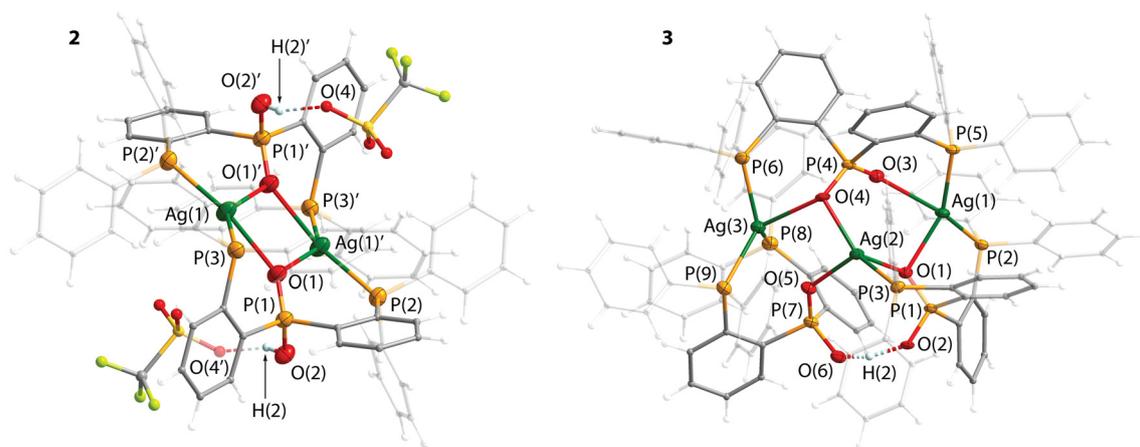
Fig. 3 Molecular views of complexes **2** and **3** obtained from SC-XRD studies. Triflate counterion in **3** is omitted for clarity. Displacement ellipsoids of non-carbon atoms are shown at the 50% probability level (CF$_3$SO$_3^-$ anions in **2** are presented in a ball-and-stick style).

This journal is © the Partner Organisations 2026

Inorg. Chem. Front., 2026, **13**, 511–524 | **515**

Fig. 4 Molecular views of complexes **4–6** (one of two independent molecules of **4** found in the unit cell is depicted, plots of **5** and **6** correspond to acetonitrile solvates). Triflate counterions and crystallization solvents are omitted for clarity. Displacement ellipsoids of non-carbon atoms are shown at the 50% probability level.

and 2.8226(6) Å for two independent molecules), despite high coordination number of one of the metal ions. Complex **4** represents one of a few cases of effective aurophilic interactions with the participation of a four-coordinated Au(I) center.[44,69,70] The P–O bonds in **4** (1.593(8)–1.597(8) Å) are visibly elongated in comparison to those in [Ag(**P³O**)] (1.5170(4) and 1.5180(4) Å) that testifies in favor of the Au⁺–PR₂–OH configuration.

The metal centers in the digold phosphinate complex **5** adopt close to linear two-coordinate geometry furnished by the P atoms of phosphine functions (Fig. 4 and Table S9), the P–Au–P motifs being nearly orthogonal to each other. Hard phosphinate donors do not participate in binding to gold(I) ions, the shortest Au⋯O distances are 2.935 and 2.771 Å (acetonitrile solvate) might suggest only weak interactions slightly distorting the P–Au–P angles (172.48(3) and 176.32(3)°). Instead, the O(1) and O(3) atoms (d(O⋯O) = 2.396(4) Å) trap the proton to form the O⋯H⋯O motif, which occupies the space between the gold centers and is sterically protected by phenyl rings.

Cluster **6** possesses a bent trigold core (∠Au(2)–Au(1)–Au(3) = 142.205(17)/144.772(8)° for diethyl ether/acetonitrile solvates) with short interatomic distances between 2.8414(5) and 2.8695(2) Å (Table S10), which are significantly below the sum of van der Waals radii (3.32 Å). Each of the lateral metal ions is decorated with two phosphine groups forming the ∠P–Au–P angle close to 170° (171.34(8)–173.23(8)°), while the central gold atom is connected to phosphide oxide anionic donors with a larger deviation from linearity (∠P(1)–Au(1)–P(4) = 168.47(8)/167.69(4)°).

As was mentioned above, cluster **6** readily co-crystallizes with complex **5**. Despite pure **5** and **6** being found in different space groups (monoclinic $P2_1/c$ and orthorhombic $Pbca$, respectively, Table S1), the similarity of structural motifs makes these cations fungible in a crystalline matrix. The formation of a solid solution of **6** in **5** was confirmed for their mixture, obtained in the course of chromatographic separation, the structure of which was satisfactorily refined as a composite containing two components with 33.3% and 66.7% occupancies (Fig. S7).

Yellowish crystals of **5***, *i.e.* **5** containing a small additive of **6**, was characterized in acetonitrile and acetone solvated forms, which are crystallographically indistinguishable from those of pure colorless **5** synthesized according to Scheme 3 (Tables S1 and S9). The powder XRD analysis also proves the crystallographic identity of bulk phases of **5** and **5*** obtained *via* two different pathways (Fig. S8), pointing to a low content of **6** embedded in the matrix of **5** (1–2% according to the NMR data, Fig. 5 and S10). Such a reproducible co-crystallization with a resolved composition of low-abundant species is rarely encountered in coordination chemistry. It reminds of the co-crystallization of dopants in organic hosts that induces room temperature phosphorescence and could lead to misinterpretation of the photophysical properties.[71,72]

In solution at room temperature, a low field signal at 18.2 ppm in the ¹H NMR spectrum of **5** (Fig. S9) matches the reported data for hydrogen-bonded homoconjugated phosphi-
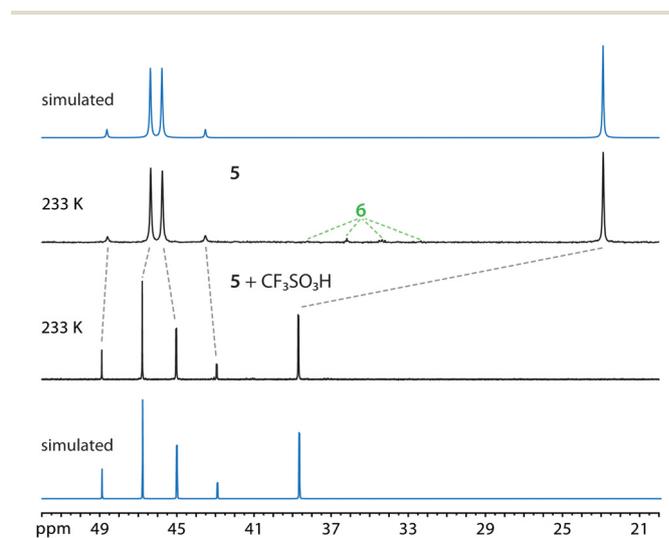
Fig. 5 162 MHz ³¹P{¹H} NMR spectra of complex **5*** before (top, showing a minor admixture of **6**) and after (bottom) addition of triflic acid (acetonitrile-d_3, 233 K).

516 | *Inorg. Chem. Front.,* 2026, **13**, 511–524

This journal is © the Partner Organisations 2026

nate ions $\{R_2POO\cdots H\cdots OOPR_2\}^{-73}$ and is consistent with this structural assignment. The phosphorus NMR spectrum of **5** shows two signals of 1 : 2 intensities ratio, assigned to POO^- (22.9 ppm) and $-PPh_2$ groups (45.7 ppm), Fig. S10. This profile purports intramolecular motion, resulting in symmetrization of the digold-diphosphine core. Below 240 K, the broad low-field singlet splits into the AB spin system P–Au–P′ ($^2J_{PP}$ = 365 Hz). The addition of an excess of triflic acid to an acetonitrile solution of **5** shifts the POO^- resonance to 38.7 ppm ($^3J_{PP}$ = 5.5 Hz at 233 K, Fig. 5) that confirms the protonation of both phosphinates. Simultaneously, it decreases the coupling within the AB system and enhances the rigidity of the complex, that is corroborated by variable temperature spectra (Fig. S10).

The ESI$^+$ mass spectra of **5** and **5** + H$^+$ display the signals of singly and doubly charged molecular cations at m/z = 1565.2 and 783.1 (Fig. S6), indicating that these species exist in dynamic equilibrium and that the dimetallic structure is retained in acidic medium. However, crystallization of **5** even in the presence of CF_3SO_3H yields only the monoprotonated form shown in Fig. 4.

The well-resolved $^{31}P\{^1H\}$ NMR spectrum of **6** at ambient temperature and the ESI$^+$-MS showing the peak of molecular ion at m/z = 1729.3 (Fig. S6) approve high structural rigidity and stability of this compound. The NMR pattern can be adequately simulated as an $X_2AA'BB'$ spin system (Fig. 6). Adding the triflic acid (3 eq.) shifts the resonance assigned to the phosphide oxide groups (δ = 82.6 ppm) to the low field region (δ = 100.4 ppm). This observation suggests the formation of phosphinous acid functions P(OH) in **6** + H$^+$ analogously to those in the protonated complex **4** bearing the same $^-P^3O$ ligand, which demonstrates a broad resonance of the P(OH) groups at δ around 101 ppm (Fig. S5). The mass spectrum of **6** in the presence of CF_3COOH shows a minor signal of dicationic species at m/z 865.1, which corresponds to the monoprotonated $[6 + H^+]^{2+}$ cluster. The loss of large coupling J_{AB} = 324 Hz in the form **6** + H$^+$ might arise from structural reorganization that nearly equivalizes phosphorus nuclei in the positions A (A′) and B′ (B).
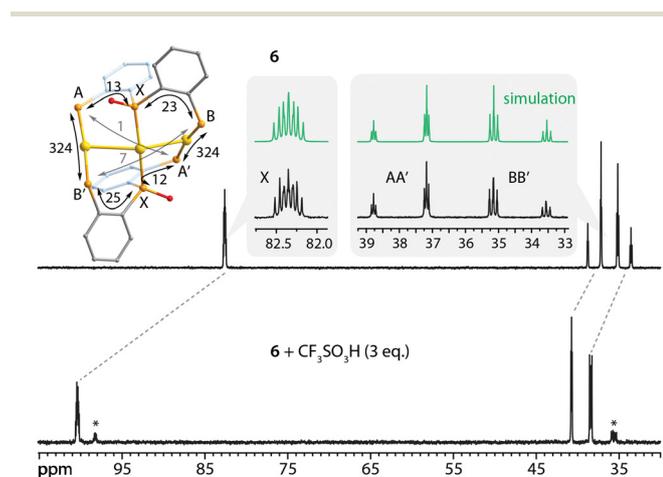

Fig. 6 202 MHz $^{31}P\{^1H\}$ NMR spectra of complex **6** before (top) and after (bottom) addition of triflic acid (acetonitrile-d_3, 297 K). The graphics show the assignment scheme and spin–spin coupling network with coupling constants (Hz) used in the simulation of the top spectrum (green profile). Minor signals indicated with asterisks could correspond to an isomeric conformation or bis-protonated species.

Photophysical properties in solution

Electronic absorption spectra of silver complexes **1**–**3** dissolved in CH_2Cl_2 show broad and featureless bands only in the UV region below 350 nm (Fig. S11), of which the lowest energy excitations are very closely spaced and dominated by MLCT Ag (d)/P(s) → aryl(π*) transitions with O(n) → aryl(π*) admixtures according to our TD-DFT calculations (Fig. 7, S12–S15 and Tables S11–S14). The digold(I) phosphinate complex **5** also exhibits intense absorptions between λ_{abs} = 300–250 nm with extinction coefficients of up to 5×10^4 M^{-1} cm^{-1} originating mainly from Au(d) → aryl(π*) MLCT and π–π* ILCT transitions occurring between the various arenes of the P^3OO- ligand, along with the depletion of electron density from oxygen atoms similarly to **1** and **2**.

Compounds **4** and **6** with aurophilic interactions extend absorption tails to longer wavelengths above 450 nm. In particular, trigold cluster **6** demonstrates a strong band peaking
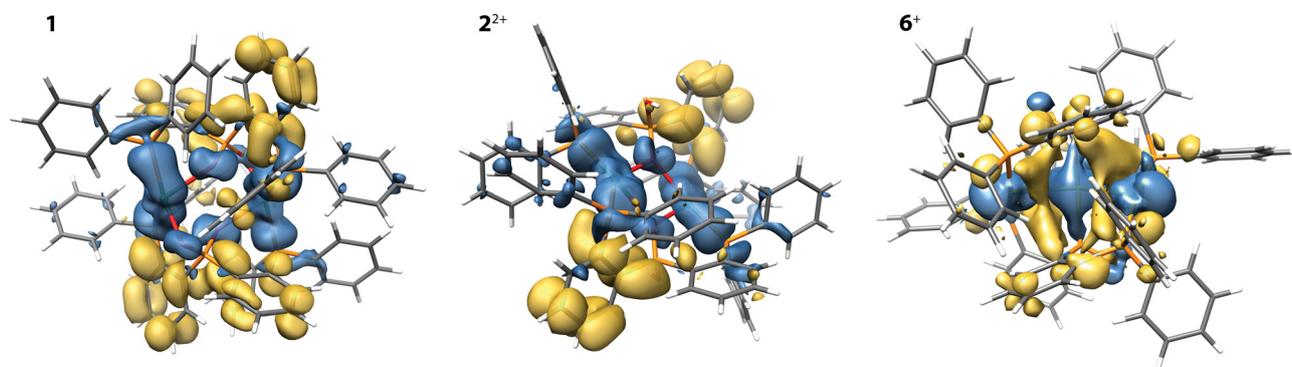
Fig. 7 Electron density difference plots for the $S_0 \rightarrow S_1$ transition from the DFT-optimized ground state of complex **1** (left), and the cations **2**$^{2+}$ (middle) and **6**$^+$ (right) obtained from TD-DFT calculations (for details, see SI; blue: loss of electron density, gold: gain of electron density).

This journal is © the Partner Organisations 2026

Inorg. Chem. Front., 2026, **13**, 511–524 | **517**

at 384 nm, which matches the predicted lowest energy singlet–singlet transition $S_0 \rightarrow S_1$ (λ = 388.7 nm, f = 0.5088, Table S14).

The S_1 state primarily involves the metal core, *i.e.* the cluster-centered (CC) configuration, supplemented with some metal-to-metal-to-ligand charge transfer, MMLCT. In addition, a weaker band is found around 440 nm (ε_{max} = 2.6 × 10^3 M^{-1} cm^{-1}) that can be assigned to direct $S_0 \rightarrow T_1$ absorption (calculated λ = 444.7 nm, Table S14 and Fig. S11) due to strong spin–orbit coupling mediated by the three gold atoms. Protonation of **6** slightly red shifts the prominent band from 384 to 390 nm (Fig. 8 and Table S15).

Among the titled complexes **1**–**6**, only cluster **6** shows detectable photoemission in solution. In dichloromethane, **6** exhibits weak blue-green luminescence with a broad band maximized at λ_{em} = 500 nm (Fig. 8 and Table S15), the low quantum yield of which Φ_{em} ∼ 0.004 did not allow for accurate determination of the excited state lifetime. Remarkably, in the presence of excess CF_3SO_3H, the emission of **6** + H$^+$ is only slightly bathochromically shifted (λ_{em} = 512 nm), but Φ_{em} is drastically enhanced (>170-fold), reaching 0.71 under oxygen-free conditions. The observed lifetime of τ = 4.0 µs and associated radiative decay rate k_r = 1.77 × 10^5 s^{-1} indicate that triplet excited states are involved either *via* phosphorescence or thermally delayed activated fluorescence (TADF). The predicted electronic configuration of the T_1 state of **6** resembles that of the S_1 (Fig. S12) and has the ^{3}CC character of the $^3[5d\sigma^*6p\sigma^1]$ type, which has been recognized as an origin of phosphorescence among di- and trinuclear gold-phosphine compounds with metal–metal bonds.[74–77] While linear chain Au$_3$ compounds can be intensely emissive in solution,[75,77] the very weak luminescence of **6** might arise from vibrational degrees of freedom of the bent trigold core.

The increase of the intensity induced by the protonation of the $^-$PO motifs (*cf.* NMR results *vide supra*) can be ascribed to the structural and electronic changes related to the $^-$PO → POH transformation, which seem to primarily suppress non-radiative relaxation that is also suggested by comparable k_r values for non-protonated **6** in crystals (see the Discussion below). Nevertheless, some acceleration of the radiative rate cannot be ruled out as evidenced by the solid-state characteristics.

Photophysical properties in the solid state

Complexes **1**–**3**, **6**, and the parent phosphine–phosphinic acid are photoluminescent in the solid state; the relevant data are listed in Table 1. Compound **5** does not show detectable emission. Neat crystals of solvated **4** demonstrate moderately intense yellow luminescence, which, however, rapidly vanishes upon drying in air and under steady-state irradiation that prevented a reliable study of this material. Under ambient conditions, ***P*^{3}*OO*H** is a weak emitter showing structureless sky-blue fluorescence (λ_{em} = 490 nm, Φ_{em} = 0.064; Fig. S16) with a nanosecond lifetime (τ_{obs} = 1.5 ns). At 77 K, the emission of the free ligand is bathochromically shifted to 547 nm and the lifetime extends to the millisecond range (τ_{av} = 12.5 ms) suggesting an interplay between singlet and triplet states, which is known to occur for compounds with acidic organophosphorus functions.[78,79]

Crystalline solvent-free **1** is a weak yellow luminophore (λ_{em} = 555 nm, Φ_{em} = 0.06). The low quantum yield of this material is caused by a high non-radiative rate (k_{nr} = 8.21 × 10^5 s^{-1}), which is nearly 17 times faster than the radiative process (k_r =
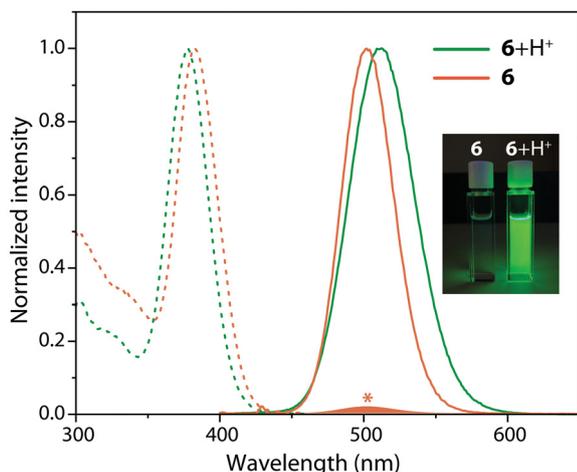
Fig. 8 UV-vis absorption (dashed lines) and emission (solid lines) spectra of complex **6** before and after the addition of excess of triflic acid, a profile indicated with an asterisk shows the relative intensity of the emission of **6** (oxygen-free dichloromethane, 297 K; insert shows a photograph of the corresponding solutions under UV light).

Table 1 Photophysical properties of ligand ***P*^{3}*OO*H** and complexes **1**–**3**, **6** and **5*** in the solid state at 297 and 77 K

	λ_{em}, nm 297 K	Φ_{em}	$\tau_{av}{}^a$, µs	$k_r \times 10^{4\,b}$, s^{-1}	$k_{nr} \times 10^{4\,c}$, s^{-1}	λ_{em}, nm 77 K	Φ_{em}	$\tau_{av}{}^a$, ms	$k_r \times 10^{2\,b}$, s^{-1}	$k_{nr} \times 10^{2\,c}$, s^{-1}
***P*^{3}*OO*H**	490	0.06	1.5 ns	4370	63 900	547	0.59	12.57	0.47	0.33
1′(MeOH)	510	0.69	19.16	3.61	1.61	511	0.99	1.58	6.25	0.06
1	555	0.06	1.15	4.87	82.1	508	—	0.49	—	—
2	514	0.44	28.61	1.54	1.96	529	0.56	2.25	2.49	1.96
3	521	0.32	6.16	5.26	11.0	522	0.74	1.28	5.78	2.04
6	488	0.76	2.53	30.0	9.49	483	—	3.21 µs	—	—
5* (5 + ∼2% **6**)	498	0.32	2.82	11.3	24.1	498	0.58	4.61 µs	1250	919

^{a} Amplitude-weighted average emission lifetime determined by the equation $\tau_{av} = \sum A_i\tau_i$, A_i = weight of the *i*-th component. ^{b} $k_r = \Phi_{em}/\tau_{av}$. ^{c} $k_{nr} = (1 - \Phi_{em})/\tau_{av}$.

518 | *Inorg. Chem. Front.*, 2026, **13**, 511–524

This journal is © the Partner Organisations 2026

4.87×10^4 s^{-1}). The neat methanol solvate **1**(MeOH), which contains 8 crystallization solvent molecules, is non-emissive, while intense green luminescence (λ_{em} = 510 nm, Φ_{em} = 0.69; Fig. 9) was observed for partially solvated **1'**(MeOH) (*vide supra*) that is readily obtained by drying **1**(MeOH) at room temperature. Intermolecular rearrangement, which occurs upon the removal of the least H-bound crystallization solvent, corresponds to the transition to another crystalline phase as evidenced by the PXRD data (Fig. S4). The elimination of the solvent-free void space likely leads to denser packing, inhibiting non-radiative relaxation, which evidently dominates for **1**(MeOH). A drastic increase of the quantum efficiency for **1'**(MeOH) *vs.* **1**, having comparable k_r values, is a manifestation of *ca.* 50-fold decelerated non-radiative rate for the former solvate ($k_{nr} = 1.61 \times 10^4$ s^{-1}). This physical behavior can be tentatively explained in terms of intramolecular structural alterations within di-(silver–phosphinate) moiety. **1'**(MeOH) presumably adopts compact and therefore stiff {Ag$_2$O$_2$} core analo-

gously to that in **1**(MeOH), which constrains excited state geometry changes and non-radiative pathways.

While the emission onsets for **1'**(MeOH) and **1** are nearly the same (Fig. 9), more severely shifted emission maximum and offset for **1** argue for pronounced structural reorganization occurring in the excited state. This feature likely reflects higher flexibility of the {Ag$_2$(OPO)$_2$} metallacyle in **1** *vs.* {Ag$_2$O$_2$} in **1'**(MeOH), which also permits more efficient non-radiative relaxation. The influence of intermolecular interactions also cannot be ruled out. The packing of **1** reveals non-negligible contacts between silver atoms and adjacent phenyl rings (Fig. S3), which can coordinate to the metals in the excited state and contribute to geometry distortions being detrimental for luminescence. A similar reason can be tentatively applied to non-emissive **1**(MeOH), which contains methanol molecules forming weak Ag⋯O contacts (3.311(3) Å, Fig. S3) and offering excessive coordination environment with additional degrees of freedom.

The photophysical characteristics of the protonated dicationic complex **2** are close to those of **1'**(MeOH). Accordingly, **2** shows green moderately intense emission (λ_{em} = 514 nm, Φ_{em} = 0.44) with a somewhat longer lifetime of 28.6 μs *cf.* 19.61 μs for **1'**(MeOH). The similar effects of protonation and hydrogen bonding on the luminescence of **1** thus primarily correlate with the structural changes of the silver-phosphinate core and its impact on the magnitude of k_{nr}, whereas the energies and localization of the electronic transitions along with the rates of ISC/radiative decay are only slightly sensitive to the degree of perturbation of the POO$^-$ groups. It is worth mentioning that packing arrangement of **2** (Fig. S3) shields the central {Ag$_2$O$_2$} core from intermolecular interactions, in contrast to the weakly and non-emissive congeners **1** and **1**(MeOH).

Trinuclear compound **3** luminesces at a longer wavelength (λ_{em} = 521 nm) and attains the fastest radiative decay among silver complexes **1–3**. However, its quantum yield of 0.32 stems from enhanced radiationless deactivation compared to dimetallic congeners **1'**(MeOH) and **2** probably due to a larger and less rigid molecular emitting core, favoring additional vibrational modes to quench the emission.

Cooling to 77 K does not change structureless emission profiles of **1–3** and induces a slight red shift of the band maxima except for solvent-free **1** (Fig. S17, Table 1). In parallel, the observed lifetimes for **1'**(MeOH), **2** and **3** are found between 1.3 and 2.2 ms, which correspond to k_r ranging from 2.49 to 6.25×10^2 s^{-1}. Such a decrease in rate constants of several orders of magnitude argues for a temperature-dependent change of the nature of the excited state and for a different emission mechanism at low temperatures, which is typically found for TADF with a Boltzmann equilibrium between, *e.g.*, $^1/$ ^{3}MLCT states. Considering relatively high quantum yields and their moderate growth under cryogenic conditions, which cannot account for the orders of magnitude change of radiative rates, monitoring of the observed lifetimes for **1'**(MeOH), **2** and **3** in the range 297–77 K was carried out in the first approximation. The obtained S-shaped temperature dependences of τ_{av} are typical of TADF materials and were satisfac-
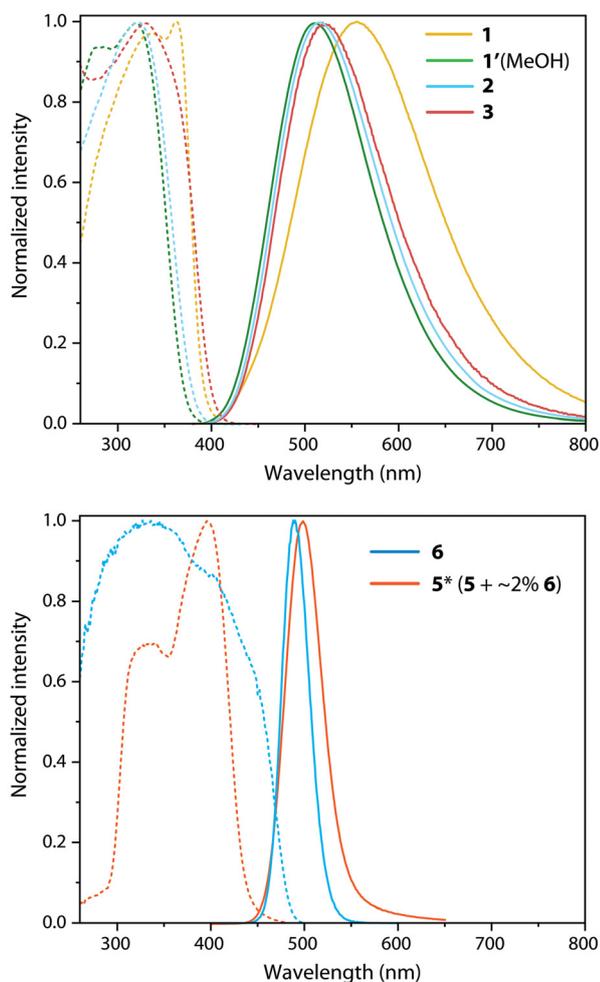
Fig. 9 Normalized excitation (dashed lines) and emission (solid lines) spectra of complexes **1–3**, **6** and **5*** (**5** doped with *ca.* 2% of **6**) in the solid state at 297 K.

This journal is © the Partner Organisations 2026

Inorg. Chem. Front., 2026, **13**, 511–524 | **519**

torily fitted using a two-state model (Fig. S18 and eqn S1). Thus, **1–3** likely realize this kind of emission process.[80] Indeed, our TD-DFT calculations of complex **1** and the dication **2**$^{2+}$ indicate energy gaps $\Delta E_{S_1 T_1}$ at the ground state geometry of 144 and 210 meV, respectively, and 190 meV for **1** at the T_1 geometry (Tables S11 and S12). These energy barriers correlate well with the experiment and appear to be small enough to be overcome at room temperature and bypass the spin-forbidden phosphorescence from the T_1 state, albeit resulting in relatively small k_r of the order of 10^4 s^{-1} in comparison to many other efficient d^{10} coinage metal TADF emitters exhibiting smaller $\Delta E_{S_1 T_1}$ and, consequently, higher values for k_r of up to 10^6 s^{-1}.[81–83]

While colorless phosphinate digold complex **5** synthesized according to Scheme 3 is not luminescent at room temperature, the phosphide oxide relative $[Au_2(\boldsymbol{P^3O})_2]$[44] and its trinuclear derivative **6** are intensely emissive in the solid state. Sky-blue luminescence of trigold cluster **6** (λ_{em} = 488 nm, Φ_{em} = 0.76) occurs at substantially higher energy than that of a yellow luminophore $[Au_2(\boldsymbol{P^3O})_2]$ (λ_{em} = 585 nm, Φ_{em} = 0.34). In contrast to broad emission profiles of $[Au_2(\boldsymbol{P^3O})_2]$ and **1–3**, **6** unveils a considerably narrower band (FWHM = 34 nm, 1412 cm^{-1} at 297 K, Fig. 9). The narrowband luminescence has been previously encountered for a few homo-[74,75,77,84] and heterometallic[85,86] gold complexes but remains rather uncommon for transition metal emitters, particularly of a multinuclear nature. The observed average lifetime for **6** exhibit a linear increase in the temperature range 297–77 K from 2.53 to 3.21 μs (Fig. S19, Table 1). Assuming that at 77 K the emission quantum yield approaches unity, k_r values are almost identical at 297 and 77 K (3.0 and 3.1 × 10^5 s^{-1}, respectively). This does not agree with the typical TADF behavior but rather suggests phosphorescence as the dominant process both at room and low temperatures. The behavior of **6** correlates with that of chain Au$_3$ clusters stabilized by tridentate phosphine[75,76] and phosphino-carbene ligands,[77] which luminesce in a blue region with quantum yields up to 0.8 and k_r reaching 3.0 × 10^5 s^{-1} in the solid state.

According to theoretical studies, the $\Delta E_{S_1 T_1}$ at the ground state geometry of the cation **6**$^+$ of 401 meV is too high to allow for TADF (Table S14). As the lowest energy triplet state T_1 is dominated by cluster-centered transitions, it is reasonable to assume that the strong SOC is mediated cooperatively by the three Au atoms and gives rise to the high phosphorescence rate constants, whereas rigid crystalline matrix diminishes nonradiative relaxation.

Unlike non-emissive pure **5**, pale-yellow crystals of **5*** (prepared as in Scheme 2) are appreciably photoluminescent. The crystallographic identity of bulk materials **5** and **5*** suggests that a minor dopant admixture is responsible for luminescence. Indeed, the crystallization of colorless **5** in the presence of 2% of **6** produces a uniform pale-yellow material with blue-greenish luminescence. This photophysical behavior is retained after several cycles of dissolving-crystallization. The emission of **6** embedded in crystals of **5** (λ_{em} = 498 nm, Table 1 and Fig. 9) is bathochromically shifted with respect to neat **6**

(λ_{em} = 488 nm) and resembles that in solution (λ_{em} = 500 nm, Table S15). A dramatic enhancement of the quantum yield in the solid vs. liquid medium (Φ_{em} = 0.32 and 0.004, respectively) is associated with minimizing radiativeless deactivations of the excited state. On the other hand, a nearly 3-fold decrease of the radiative rate for **6** in **5** vs. neat **6** (k_r = 1.1 × 10^5 and 3.0 × 10^5 s^{-1}, respectively) suggests non-negligible roles of intermolecular interactions and intramolecular geometry alterations (e.g. the angle and distances within the Au$_3$ core) imposed by different matrices in affecting the SOC and the probabilities of spin-forbidden transitions.

Conclusions

In this work, we combined a phosphinic group with phosphine functions to give a hybrid chelating ligand $\boldsymbol{P^3OO}$H, which was used for the preparation of a disilver complex **1**. The phosphinate residue R$_2$PO$_2^-$ readily forms hydrogen bonds or undergoes protonation. Both interactions have conceptually similar influence on coordination mode of the ligand to silver centers and reversibly alter molecular arrangement yielding dimetallic compounds **1**(MeOH), **2**, and a trinuclear cluster **3**, regulated by the degree of protonation. Furthermore, structural variation affects photoluminescence behavior of the titled species, likely showing TADF property. While emission energies of **1–3** have rather moderate dependence on structural features, the P–O···H interactions and intermolecular packing govern the rates of non-radiative decay, resulting in variations of the quantum yield from 0.06 up to 0.69 in the solid state. Opposite to **1** and **2**, the non-luminescent digold relative **5** can be isolated only in a monoprotonated form, which is further readily protonated in solution with the suppression of intramolecular dynamics.

We have also investigated the behavior of congener disilver (I) and digold(I) complexes comprising phosphine–phosphide oxide ligand $^-\boldsymbol{P^3O}$ towards acids, which are capable of promoting oxidation of the coordinated $^-$P=O group to the phosphinic acid to generate compounds **2** and **5** from $[M_2(\boldsymbol{P^3O})_2]$ precursors. Notably, it was shown that the synthesis of **5** via acid-mediated protocol affords a minor co-product, a trigold complex **6**, which co-crystallizes very efficiently with **5** due to their structural similarity to form a solid solution of **6** in **5** (**5***) with bright luminescence even at low doping concentrations of 1–2%. Compound **6** can be selectively derived from $[Au_2(\boldsymbol{P^3O})_2]$ in a reaction of cluster expansion. The phosphide oxide function in **6** is stabilized by the additional gold center towards the oxidation and endures protonation with a dramatic enhancement of the intensity of the phosphorescence in solution. In the solid state, cluster **6** is the brightest emitter among studied complexes with the quantum yield of 0.76.

The difficulty in evaluating a minor admixture underscores surprising formal interchangeability O···H···O ↔ Au that occurs within these ligand environments and simultaneously illustrates new possibilities for the design of new light emitting molecular materials of coinage metal complexes.

520 | *Inorg. Chem. Front.*, 2026, **13**, 511–524

This journal is © the Partner Organisations 2026

Author contributions

M. B., A. B., H. K., J. J., and O. M. performed experimental investigations (M. B.: most of the syntheses, structural and spectroscopic characterization; A. B. and H. K.: synthesis and photophysical studies; J. J.: mass-spectroscopic measurements). O. M. and A. S. carried out computational analysis. A. S. and I. O. K. carried out supervision of the project. M. B., A. S. and I. O. K. wrote the manuscript. All authors approved the final version of the manuscript.

Conflicts of interest

There are no conflicts to declare.

Data availability

The raw data is available from authors on request.

Supplementary information (SI): experimental procedures and computational studies. See DOI: https://doi.org/10.1039/d5qi01622c.

CCDC 2475264–2475275 (**1–6** and P^3OOH) contain the supplementary crystallographic data for this paper.[87a–l]

Acknowledgements

References

1 A. Steinegger, O. S. Wolfbeis and S. M. Borisov, Optical Sensing and Imaging of pH Values: Spectroscopies, Materials, and Applications, *Chem. Rev.*, 2020, **120**, 12357–12489.

2 Z. Deng, C. Wang, H. Zhang, T. Ai and K. Kou, Hydrogen-Bonded Colorimetric and Fluorescence Chemosensor for Fluoride Anion With High Selectivity and Sensitivity: A Review, *Front. Chem.*, 2021, **9**, 666450.

3 E. A. Kataev, Converting pH probes into "turn-on" fluorescent receptors for anions, *Chem. Commun.*, 2023, **59**, 1717–1727.

4 S.-S. Xue, Y. Li, W. Pan, N. Li and B. Tang, Multi-stimuli-responsive molecular fluorescent probes for bioapplications, *Chem. Commun.*, 2023, **59**, 3040–3049.

5 I. Aprahamian, Hydrazone switches and things in between, *Chem. Commun.*, 2017, **53**, 6674–6684.

6 Y. Zhang, S. Tang, E. R. Thapaliya, L. Sansalone and F. M. Raymo, Fluorescence activation with switchable oxazines, *Chem. Commun.*, 2018, **54**, 8799–8809.

7 Y. Wang, Y.-M. Zhang and S. X.-A. Zhang, Stimuli-Induced Reversible Proton Transfer for Stimuli-Responsive Materials and Devices, *Acc. Chem. Res.*, 2021, **54**, 2216–2226.

8 J. Zhang, B. He, Y. Hu, P. Alam, H. Zhang, J. W. Y. Lam and B. Z. Tang, Stimuli-Responsive AIEgens, *Adv. Mater.*, 2021, **33**, 2008071.

9 G.-J. Zhao and K.-L. Han, Hydrogen Bonding in the Electronic Excited State, *Acc. Chem. Res.*, 2012, **45**, 404–413.

10 M. V. Werrett, S. Muzzioli, P. J. Wright, A. Palazzi, P. Raiteri, S. Zacchini, M. Massi and S. Stagni, Proton-Induced Reversible Modulation of the Luminescent Output of Rhenium(I), Iridium(III), and Ruthenium(II) Tetrazolate Complexes, *Inorg. Chem.*, 2014, **53**, 229–243.

11 K. M.-C. Wong, W.-S. Tang, X.-X. Lu, N. Zhu and V. W.-W. Yam, Functionalized Platinum(II) Terpyridyl Alkynyl Complexes as Colorimetric and Luminescence pH Sensors, *Inorg. Chem.*, 2005, **44**, 1492–1498.

12 A. Nakagawa, Y. Hisamatsu, S. Moromizato, M. Kohno and S. Aoki, Synthesis and Photochemical Properties of pH Responsive Tris-Cyclometalated Iridium(III) Complexes That Contain a Pyridine Ring on the 2-Phenylpyridine Ligand, *Inorg. Chem.*, 2014, **53**, 409–422.

13 Y. Ma, H. Liang, Y. Zeng, H. Yang, C.-L. Ho, W. Xu, Q. Zhao, W. Huang and W.-Y. Wong, Phosphorescent soft salt for ratiometric and lifetime imaging of intracellular pH variations, *Chem. Sci.*, 2016, **7**, 3338–3346.

14 K. Qiu, L. Ke, X. Zhang, Y. Liu, T. W. Rees, L. Ji, J. Diao and H. Chao, Tracking mitochondrial pH fluctuation during cell apoptosis with two-photon phosphorescent iridium(III) complexes, *Chem. Commun.*, 2018, **54**, 2421–2424.

15 N. S. Y. Abdolla, D. L. Davies, M. P. Lowe and K. Singh, Bis-cyclometallated Ir(iii) complexes containing 2-(1H-pyrazol-3-yl)pyridine ligands; influence of substituents and cyclometallating ligands on response to changes in pH, *Dalton Trans.*, 2020, **49**, 12025–12036.

16 Z. Han, Y. Wang, Y. Chen, H. Fang, H. Yuan, X. Shi, B. Yang, Z. Chen, W. He and Z. Guo, A novel luminescent Ir(III) complex for dual mode imaging: synergistic response to hypoxia and acidity of the tumor microenvironment, *Chem. Commun.*, 2020, **56**, 8055–8058.

17 J. R. Shakirova, V. A. Baigildin, A. I. Solomatina, R. B. Aghakhanpour, V. V. Pavlovskiy, V. V. Porsev and S. P. Tunik, Intracellular pH Sensor Based on Heteroleptic Bis-Cyclometalated Iridium(III) Complex Embedded into Block-Copolymer Nanospecies: Application in Phosphorescence Lifetime Imaging Microscopy, *Adv. Funct. Mater.*, 2023, **33**, 2212390.

This journal is © the Partner Organisations 2026

Inorg. Chem. Front., 2026, **13**, 511–524 | **521**

18 K. Li, Y. Chen, W. Lu, N. Zhu and C.-M. Che, A Cyclometalated Platinum(II) Complex with a Pendent Pyridyl Motif as Solid-State Luminescent Sensor for Acidic Vapors, *Chem. – Eur. J.*, 2011, **17**, 4109–4112.

19 D. Li, G. Li, W. Che, D. Zhu and Z. Su, A remarkable phosphorescent sensor for acid–base vapours based on an AIPE-active Ir(III) complex, *Dalton Trans.*, 2019, **48**, 1955–1959.

20 S. Miyamoto, K. Nagata and T. Yoshimura, Luminescence Color and Intensity Changes of Nitridorhenium(V) Complexes Induced by Protonation/Deprotonation on the Bidentate Azolylpyridine Ligands, *Inorg. Chem.*, 2023, **62**, 17641–17653.

21 D. Qiu, M. Li, Q. Zhao, H. Wang and C. Yang, Cyclometalated Platinum(II) Terpyridylacetylide with a Bis (arylamine) Donor as a Proton-Triggered Luminescence Chemosensor for Zn2+, *Inorg. Chem.*, 2015, **54**, 7774–7782.

22 S.-S. Sun, A. J. Lees and P. Y. Zavalij, Highly Sensitive Luminescent Metal-Complex Receptors for Anions through Charge-Assisted Amide Hydrogen Bonding, *Inorg. Chem.*, 2003, **42**, 3445–3453.

23 S. A. Rommel, D. Sorsche and S. Rau, A supramolecular H-bond driven light switch sensor for small anions, *Dalton Trans.*, 2016, **45**, 74–77.

24 P. Yang, S. Zhang, K. Wang and H. Qi, Synthesis of pH-responsive cyclometalated iridium(III) complex and its application in the selective killing of cancerous cells, *Dalton Trans.*, 2021, **50**, 17338–17345.

25 M. Kato, S. Kishi, Y. Wakamatsu, Y. Sugi, Y. Osamura, T. Koshiyama and M. Hasegawa, Outstanding Vapochromism and pH-dependent Coloration of Dicyano(4,4′-dicarboxy-2,2′-bipyridine)platinum(II) with a Three-dimensional Network Structure, *Chem. Lett.*, 2005, **34**, 1368–1369.

26 C.-K. Koo, B. Lam, S.-K. Leung, M. H.-W. Lam and W.-Y. Wong, A "Molecular Pivot-Hinge" Based on the pH-Regulated Intramolecular Switching of Pt–Pt and π–π Interactions, *J. Am. Chem. Soc.*, 2006, **128**, 16434–16435.

27 J. L.-L. Tsai, T. Zou, J. Liu, T. Chen, A. O.-Y. Chan, C. Yang, C.-N. Lok and C.-M. Che, Luminescent platinum(II) complexes with self-assembly and anti-cancer properties: hydrogel, pH dependent emission color and sustained-release properties under physiological conditions, *Chem. Sci.*, 2015, **6**, 3823–3830.

28 Z. Chen, M. H.-Y. Chan and V. W.-W. Yam, Stimuli-Responsive Two-Dimensional Supramolecular Polymers Based on Trinuclear Platinum(II) Scaffolds: Reversible Modulation of Photoluminescence, Cavity Size, and Water Permeability, *J. Am. Chem. Soc.*, 2020, **142**, 16471–16478.

29 X. Meng, T. Moriuchi, M. Kawahata, K. Yamaguchi and T. Hirao, A G-octamer scaffold viaself-assembly of a guanosine-based Au(I) isonitrile complex for Au(I)–Au(I) interaction, *Chem. Commun.*, 2011, **47**, 4682–4684.

30 I. O. Koshevoy, C.-L. Lin, A. J. Karttunen, J. Jänis, M. Haukka, S. P. Tunik, P.-T. Chou and T. A. Pakkanen, Highly luminescent octanuclear AuI-CuI clusters adopting two structural motifs: the effect of aliphatic alkynyl ligands, *Chem. – Eur. J.*, 2011, **17**, 11456–11466.

31 M. Ebina, A. Kobayashi, T. Ogawa, M. Yoshida and M. Kato, Impact of a Carboxyl Group on a Cyclometalated Ligand: Hydrogen-Bond- and Coordination-Driven Self-Assembly of a Luminescent Platinum(II) Complex, *Inorg. Chem.*, 2015, **54**, 8878–8880.

32 M. J. Bryant, J. M. Skelton, L. E. Hatcher, C. Stubbs, E. Madrid, A. R. Pallipurath, L. H. Thomas, C. H. Woodall, J. Christensen, S. Fuertes, T. P. Robinson, C. M. Beavers, S. J. Teat, M. R. Warren, F. Pradaux-Caggiano, A. Walsh, F. Marken, D. R. Carbery, S. C. Parker, N. B. McKeown, R. Malpass-Evans, M. Carta and P. R. Raithby, A rapidly-reversible absorptive and emissive vapochromic Pt(II) pincer-based chemical sensor, *Nat. Commun.*, 2017, **8**, 1800.

33 Y. Shigeta, A. Kobayashi, M. Yoshida and M. Kato, Crystal Engineering of Vapochromic Porous Crystals Composed of Pt(II)-Diimine Luminophores for Vapor-History Sensors, *Cryst. Growth Des.*, 2018, **18**, 3419–3427.

34 A. Kobayashi, N. Yamamoto, Y. Shigeta, M. Yoshida and M. Kato, Two-way vapochromism of a luminescent platinum(II) complex with phosphonic-acid-functionalized bipyridine ligand, *Dalton Trans.*, 2018, **47**, 1548–1556.

35 K. Ohno, Y. Kusano, S. Kaizaki, A. Nagasawa and T. Fujihara, Chromism of Tartrate-Bridged Clamshell-like Platinum(II) Complex: Intramolecular Pt–Pt Interaction-Induced Luminescence Vapochromism and Intermolecular Interactions-Triggered Thermochromism, *Inorg. Chem.*, 2018, **57**, 14159–14169.

36 D. Blasco, J. M. López-de-Luzuriaga, M. Monge, M. E. Olmos, D. Pascual and M. Rodríguez-Castillo, Time-Dependent Molecular Rearrangement of [Au(N9-adeninate) (PTA)] in Aqueous Solution and Aggregation-Induced Emission in a Hydrogel Matrix, *Inorg. Chem.*, 2021, **60**, 3667–3676.

37 P. Braunstein and F. Naud, Hemilability of hybrid ligands and the coordination chemistry of oxazoline-based systems, *Angew. Chem., Int. Ed.*, 2001, **40**, 680–699.

38 S. E. Angell, C. W. Rogers, Y. Zhang, M. O. Wolf and W. E. J. Jones, Hemilabile coordination complexes for sensing applications, *Coord. Chem. Rev.*, 2006, **250**, 1829–1841.

39 G. M. Adams and A. S. Weller, POP-type ligands: Variable coordination and hemilabile behaviour, *Coord. Chem. Rev.*, 2018, **355**, 150–172.

40 B. Higgins, B. A. DeGraff and J. N. Demas, Luminescent Transition Metal Complexes as Sensors: Structural Effects on pH Response, *Inorg. Chem.*, 2005, **44**, 6662–6669.

41 D. Sun, Z.-H. Wei, C.-F. Yang, D.-F. Wang, N. Zhang, R.-B. Huang and L.-S. Zheng, pH-Dependent Ag(I) coordination architectures constructed from 4-cyanopyridine and phthalic acid: from discrete structure to 2D sheet, *CrystEngComm*, 2011, **13**, 1591–1601.

42 T. M. Dau, B. D. Asamoah, A. Belyaev, G. Chakkaradhari, P. Hirva, J. Jänis, E. V. Grachova, S. P. Tunik and I. O. Koshevoy, Adjustable coordination of a hybrid phosphine-phosphine oxide ligand in luminescent Cu, Ag and Au complexes, *Dalton Trans.*, 2016, **45**, 14160–14173.

522 | *Inorg. Chem. Front.*, 2026, **13**, 511–524

This journal is © the Partner Organisations 2026

43 M. Beliaeva, A. Belyaev, E. V. Grachova, A. Steffen and I. O. Koshevoy, Ditopic phosphide oxide group: a rigidifying Lewis base to switch luminescence and reactivity of a disilver complex, *J. Am. Chem. Soc.*, 2021, **143**, 15045–15055.

44 M. Beliaeva, A. Belyaev, A. Steffen and I. O. Koshevoy, Cluster expansion of luminescent digold(I) and disilver(I) phosphine-phosphide oxide complexes, *Inorg. Chem.*, 2025, **64**, 14513–14523.

45 E. R. T. Tiekink and J.-G. Kang, Luminescence Properties of Phosphinegold(I) Halides and Thiolates, *Coord. Chem. Rev.*, 2009, **253**, 1627–1648.

46 V. W.-W. Yam, V. K.-M. Au and S. Y.-L. Leung, Light-Emitting Self-Assembled Materials Based on d^8 and d^{10} Transition Metal Complexes, *Chem. Rev.*, 2015, **115**, 7589–7728.

47 H. Yersin, R. Czerwieniec, M. Z. Shafikov and A. F. Suleymanova, TADF Material Design: Photophysical Background and Case Studies Focusing on CuI and AgI Complexes, *ChemPhysChem*, 2017, **18**, 3508–3535.

48 M. Pujadas and L. Rodríguez, Luminescent phosphine gold (I) alkynyl complexes. Highlights from 2010 to 2018, *Coord. Chem. Rev.*, 2020, **408**, 213179.

49 A. V. Paderina, I. O. Koshevoy and E. V. Grachova, Keep it tight: a crucial role of bridging phosphine ligands in the design and optical properties of multinuclear coinage metal complexes, *Dalton Trans.*, 2021, **50**, 6003–6033.

50 L. C. Thomas, R. A. Chittenden and H. E. R. Hartley, Hydrogen Bonding in Alkyl Phosphonic and Alkyl Phosphonothionic Acids, *Nature*, 1961, **192**, 1283–1284.

51 J. A. Walmsley, Self-association of phosphinic acids in non-polar solvents. The origin of the apparent dipole moment in symmetric dimers, *J. Phys. Chem.*, 1984, **88**, 1226–1231.

52 M. A. Carvajal, J. J. Novoa and S. Alvarez, Choice of Coordination Number in d10 Complexes of Group 11 Metals, *J. Am. Chem. Soc.*, 2004, **126**, 1465–1477.

53 R. A. Baldwin, M. T. Cheng and G. D. Homer, Application of the Hammett equation to organophosphorus-substituted phosphinic and benzoic acids, *J. Org. Chem.*, 1967, **32**, 2176–2180.

54 P. Machnitzki, T. Nickel, O. Stelzer and C. Landgrafe, Novel Syntheses of Mono- and Bisphosphonated Aromatic Phosphanes by Consecutive Pd-Catalyzed P–C Coupling Reactions and Nucleophilic Phosphanylation – X-ray Structure of $Ph_2P\text{-}C_6H_4\text{-}m\text{-}PO_3Na_2\cdot5.5H_2O$ · *i*PrOH, *Eur. J. Inorg. Chem.*, 1998, 1029–1034.

55 W. J. Dressick, C. George, S. L. Brandow, T. L. Schull and D. A. Knight, Convenient Synthesis of the Water-Soluble Ligand Hexasodium Tris(4-phosphonatophenyl)phosphine, *J. Org. Chem.*, 2000, **65**, 5059–5062.

56 T. L. Schull, J. C. Fettinger and D. A. Knight, Synthesis and Characterization of Palladium(II) and Platinum(II) Complexes Containing Water-Soluble Hybrid Phosphine–Phosphonate Ligands, *Inorg. Chem.*, 1996, **35**, 6717–6723.

57 C. M. Reisinger, R. J. Nowack, D. Volkmer and B. Rieger, Novel palladium complexes employing mixed phosphine phosphonates and phosphine phosphinates as anionic chelating [P,O] ligands, *Dalton Trans.*, 2007, 272–278.

58 T. L. Schull, L. Henley, J. R. Deschamps, R. J. Butcher, D. P. Maher, C. A. Klug, K. Swider-Lyons, W. J. Dressick, B. Bujoli, A. E. Greenwood, L. K. B. Congiardo and D. A. Knight, Organometallic Supramolecular Mixed-Valence Cobalt(I)/Cobalt(II) Aquo Complexes Stabilized with the Water-Soluble Phosphine Ligand p-TPPTP (p-triphenyl-phosphine triphosphonic acid), *Organometallics*, 2007, **26**, 2272–2276.

59 A. M. Wilders, N. D. Contrella, J. R. Sampson, M. Zheng and R. F. Jordan, Allosteric Effects in Ethylene Polymerization Catalysis. Enhancement of Performance of Phosphine-Phosphinate and Phosphine-Phosphonate Palladium Alkyl Catalysts by Remote Binding of $B(C_6F_5)_3$, *Organometallics*, 2017, **36**, 4990–5002.

60 N. Glebko, T. M. Dau, A. S. Melnikov, E. V. Grachova, I. V. Solovyev, A. Belyaev, A. J. Karttunen and I. O. Koshevoy, Luminescence thermochromism of gold(I) phosphane-iodide complexes: a rule or an exception?, *Chem. – Eur. J.*, 2018, **24**, 3021–3029.

61 X. Tan, W. Zeng, X. Zhang, L. W. Chung and X. Zhang, Development of a novel secondary phosphine oxide–ruthenium(II) catalyst and its application for carbonyl reduction, *Chem. Commun.*, 2018, **54**, 535–538.

62 B. K. Teo, Y. H. Xu, B. Y. Zhong, Y. K. He, H. Y. Chen, W. Qian, Y. J. Deng and Y. H. Zou, A Comparative Study of Third-Order Nonlinear Optical Properties of Silver Phenylacetylide and Related Compounds via Ultrafast Optical Kerr Effect Measurements, *Inorg. Chem.*, 2001, **40**, 6794–6801.

63 Y. Takemura, T. Nakajima and T. Tanase, Synthesis and Characterization of Linear Tetranuclear Silver(I) Complexes Bridged by Tetraphosphane Ligands, *Eur. J. Inorg. Chem.*, 2009, 4820–4829.

64 M.-Q. He, Y. Xu, M.-X. Li, M. Shao and Z.-X. Wang, Various Silver Phosphinate Inorganic Architectures in Three-Dimensional Frameworks with Argentophilic Interactions, *Cryst. Growth Des.*, 2019, **19**, 2892–2898.

65 J. Wei, F. Bigdeli, L.-X. Wang, L.-L. Hou, A. Panjehpour, Y. Ma, K.-Z. Wang, A. Morsali and K.-G. Liu, Template-Free Synthesis of Two New Luminescent One-Dimensional High-Nuclearity Silver Polyclusters, *Inorg. Chem.*, 2023, **62**, 10185–10192.

66 M. Osawa, M. Hashimoto, I. Kawata and M. Hoshino, Photoluminescence properties of TADF-emitting three-coordinate silver(I) halide complexes with diphosphine ligands: a comparison study with copper(I) complexes, *Dalton Trans.*, 2017, **46**, 12446–12455.

67 H. Schmidbaur and A. Schier, Argentophilic Interactions, *Angew. Chem., Int. Ed.*, 2015, **54**, 746–784.

68 S. Alvarez, A cartography of the van der Waals territories, *Dalton Trans.*, 2013, **42**, 8617–8636.

69 J. Zank, A. Schier and H. Schmidbaur, Gold and silver cations in the "Procrustean Bed" of the bis[2-(diphenylphosphino)phenyl]phenylphosphine ligand. Observations and conclusions, *J. Chem. Soc., Dalton Trans.*, 1999, 415–420.

70 A. Maspero, I. Kani, A. A. Mohamed, M. A. Omary, R. J. Staples and J. P. Fackler, Syntheses and Structures of

Dinuclear Gold(ɪ) Dithiophosphonate Complexes and the Reaction of the Dithiophosphonate Complexes with Phosphines: Diverse Coordination Types, *Inorg. Chem.*, 2003, **42**, 5311–5319.

71 C. Chen, Z. Chi, K. C. Chong, A. S. Batsanov, Z. Yang, Z. Mao, Z. Yang and B. Liu, Carbazole isomers induce ultralong organic phosphorescence, *Nat. Mater.*, 2021, **20**, 175–180.

72 Z. Wu, K. Bergmann and Z. M. Hudson, Dopants Induce Persistent Room Temperature Phosphorescence in Triarylamine Boronate Esters, *Angew. Chem., Int. Ed.*, 2024, **63**, e202319089.

73 C. Detering, P. M. Tolstoy, N. S. Golubev, G. S. Denisov and H. H. Limbach, Vicinal H/D Isotope Effects in NMR Spectra of Complexes with Coupled Hydrogen Bonds: Phosphoric Acids, *Dokl. Phys. Chem.*, 2001, **379**, 191–193.

74 W.-F. Fu, K.-C. Chan, K.-K. Cheung and C.-M. Che, Substrate-Binding Reactions of the $^3[d\sigma^*p\sigma]$ Excited State of Binuclear Gold(ɪ) Complexes with Bridging Bis(dicyclohexylphosphino)methane Ligands: Emission and Time-Resolved Absorption Spectroscopic Studies, *Chem. – Eur. J.*, 2001, **7**, 4656–4664.

75 G. S. M. Tong, S. C. F. Kui, H.-Y. Chao, N. Zhu and C.-M. Che, The $^3[nd\sigma^*(n+1)p\sigma]$ Emissions of Linear Silver(ɪ) and Gold(ɪ) Chains with Bridging Phosphine Ligands, *Chem. – Eur. J.*, 2009, **15**, 10777–10789.

76 T. M. Dau, J. R. Shakirova, A. J. Karttunen, E. V. Grachova, S. P. Tunik, A. S. Melnikov, T. A. Pakkanen and I. O. Koshevoy, Coinage metal complexes supported by the tri- and tetraphosphine ligands, *Inorg. Chem.*, 2014, **53**, 4705–4715.

77 P. Ai, M. Mauro, C. Gourlaouen, S. Carrara, L. De Cola, Y. Tobon, U. Giovanella, C. Botta, A. A. Danopoulos and P. Braunstein, Bonding, Luminescence, Metallophilicity in Linear Au_3 and Au_2Ag Chains Stabilized by Rigid Diphosphanyl NHC Ligands, *Inorg. Chem.*, 2016, **55**, 8527–8542.

78 S. Jena, A. T. Muhammed Munthasir and P. Thilagar, Unraveling Ultralong Phosphorescence in $Ar_2PO(H)$: $n(O) \rightarrow \sigma^*(P-C)$ Transitions in $Ar_2PO(H)$ Stabilize Triplet States Better than $n(P) \rightarrow \sigma^*(P-C)$ in Ar_3P, *J. Phys. Chem. C*, 2023, **127**, 9918–9930.

79 N. Ledos, D. Jacquemin, P.-A. Bouit and M. Hissler, Exploiting P-chemistry to modulate the thermally activated delayed fluorescence of organic fluorophores, *Dyes Pigm.*, 2024, **224**, 111978.

80 R. Czerwieniec, M. J. Leitl, H. H. H. Homeier and H. Yersin, Cu(ɪ) complexes – Thermally activated delayed fluorescence. Photophysical approach and material design, *Coord. Chem. Rev.*, 2016, **325**, 2–28.

81 R. Hamze, S. Shi, S. C. Kapper, D. S. Muthiah Ravinson, L. Estergreen, M.-C. Jung, A. C. Tadle, R. Haiges,

P. I. Djurovich, J. L. Peltier, R. Jazzar, G. Bertrand, S. E. Bradforth and M. E. Thompson, "Quick-Silver" from a Systematic Study of Highly Luminescent, Two-Coordinate, d^{10} Coinage Metal Complexes, *J. Am. Chem. Soc.*, 2019, **141**, 8616–8626.

82 J. Ma, J. Schaab, S. Paul, S. R. Forrest, P. I. Djurovich and M. E. Thompson, Luminescent Bimetallic Two-Coordinate Gold(ɪ) Complexes Utilizing Janus Carbenes, *J. Am. Chem. Soc.*, 2023, **145**, 20097–20108.

83 A. Ying, N. Li, X. Chen, J. Xia, C. Yang and S. Gong, Ag(ɪ) emitters with ultrafast spin-flip dynamics for high-efficiency electroluminescence, *Chem. Sci.*, 2025, **16**, 784–792.

84 R. Hamze, M. Idris, D. S. Muthiah Ravinson, M. C. Jung, R. Haiges, P. I. Djurovich and M. E. Thompson, Highly Efficient Deep Blue Luminescence of 2-Coordinate Coinage Metal Complexes Bearing Bulky NHC Benzimidazolyl Carbene, *Front. Chem.*, 2020, **8**, 401.

85 N. Natarajan, L.-X. Shi, H. Xiao, J.-Y. Wang, L.-Y. Zhang, X. Zhang and Z.-N. Chen, $PtAu_3$ cluster complexes with narrow-band emissions for solution-processed organic light emitting diodes, *J. Mater. Chem. C*, 2019, **7**, 2604–2614.

86 D.-S. Zheng, J.-Y. Wang, L.-X. Shi and Z.-N. Chen, Modulating Narrow-Band Phosphorescence of Pt_2Au_4 Cluster Complexes by Differently Positioned Bis(acetylide)-Naphthalene Linkers, *ACS Appl. Electron. Mater.*, 2023, **5**, 994–1001.

87 (*a*) CCDC 2475264: Experimental Crystal Structure Determination, 2025, DOI: **10.5517/ccdc.csd.cc2p2q7r**; (*b*) CCDC 2475265: Experimental Crystal Structure Determination, 2025, DOI: **10.5517/ccdc.csd.cc2p2q8s**; (*c*) CCDC 2475266: Experimental Crystal Structure Determination, 2025, DOI: **10.5517/ccdc.csd.cc2p2q9t**; (*d*) CCDC 2475267: Experimental Crystal Structure Determination, 2025, DOI: **10.5517/ccdc.csd.cc2p2qbv**; (*e*) CCDC 2475268: Experimental Crystal Structure Determination, 2025, DOI: **10.5517/ccdc.csd.cc2p2qcw**; (*f*) CCDC 2475269: Experimental Crystal Structure Determination, 2025, DOI: **10.5517/ccdc.csd.cc2p2qdx**; (*g*) CCDC 2475270: Experimental Crystal Structure Determination, 2025, DOI: **10.5517/ccdc.csd.cc2p2qfy**; (*h*) CCDC 2475271: Experimental Crystal Structure Determination, 2025, DOI: **10.5517/ccdc.csd.cc2p2qgz**; (*i*) CCDC 2475272: Experimental Crystal Structure Determination, 2025, DOI: **10.5517/ccdc.csd.cc2p2qh0**; (*j*) CCDC 2475273: Experimental Crystal Structure Determination, 2025, DOI: **10.5517/ccdc.csd.cc2p2qj1**; (*k*) CCDC 2475274: Experimental Crystal Structure Determination, 2025, DOI: **10.5517/ccdc.csd.cc2p2qk2**; (*l*) CCDC 2475275: Experimental Crystal Structure Determination, 2025, DOI: **10.5517/ccdc.csd.cc2p2ql3**.

524 | *Inorg. Chem. Front.*, 2026, **13**, 511–524

This journal is © the Partner Organisations 2026